

# Post-Training Quantization for Video Matting

Tianrui Zhu<sup>1</sup>   Houyuan Chen<sup>1</sup>   Ruihao Gong<sup>2</sup>  
 Michele Magno<sup>3</sup>   Haotong Qin<sup>3\*</sup>   Kai Zhang<sup>1\*</sup>  
<sup>1</sup>Nanjing University   <sup>2</sup>SenseTime Research   <sup>3</sup>ETH Zürich

## Abstract

Video matting is crucial for applications such as film production and virtual reality, yet deploying its computationally intensive models on resource-constrained devices presents challenges. Quantization is a key technique for model compression and acceleration. As an efficient approach, Post-Training Quantization (PTQ) is still in its nascent stages for video matting, facing significant hurdles in maintaining accuracy and temporal coherence. To address these challenges, this paper proposes a novel and general PTQ framework specifically designed for video matting models, marking, to the best of our knowledge, the first systematic attempt in this domain. Our contributions include: (1) A two-stage PTQ strategy that combines block-reconstruction-based optimization for fast, stable initial quantization and local dependency capture, followed by a global calibration of quantization parameters to minimize accuracy loss. (2) A Statistically-Driven Global Affine Calibration (GAC) method that enables the network to compensate for cumulative statistical distortions arising from factors such as neglected BN layer effects, even reducing the error of existing PTQ methods on video matting tasks up to 20%. (3) An Optical Flow Assistance (OFA) component that leverages temporal and semantic priors from frames to guide the PTQ process, enhancing the model’s ability to distinguish moving foregrounds in complex scenes and ultimately achieving near full-precision performance even under ultra-low-bit quantization. Comprehensive quantitative and visual results show that our PTQ4VM achieves the state-of-the-art accuracy performance across different bit-widths compared to the existing quantization methods. We highlight that the 4-bit PTQ4VM even achieves performance close to the full-precision counterpart while enjoying  $8\times$  FLOP savings.

## 1 Introduction

The purpose of video matting [2, 3, 4, 5, 6, 7, 10, 1, 11, 8, 9, 15, 13, 16, 14, 12, 17] is to accurately estimate the alpha matte ( $\alpha \in [0, 1]$ ) of the foreground objects for each frame in a video sequence. The alpha matte defines the foreground opacity at each pixel, governed by the compositing equation  $I = \alpha F + (1 - \alpha)B$ , where  $I$  is the observed pixel,  $F$  is the foreground, and  $B$  is the background. This challenging computer vision task has broad applications in film production, video conferencing, virtual reality, and more. To enable real-time performance and deployment on resource-constrained platforms for these diverse applications, efficient model representations are crucial. This necessitates advanced model compression techniques to reduce the computational and memory footprint of video matting models, making them suitable for edge computing devices.

Model compression techniques, particularly quantization [18, 19, 20], are paramount for deploying advanced video matting models on resource-constrained devices by converting high-precision floating-point numbers to low-bit integers, thereby reducing model size and accelerating computation. While Quantization-Aware Training [35](QAT) simulates quantization during training to achieve good

---

\*Corresponding authors.

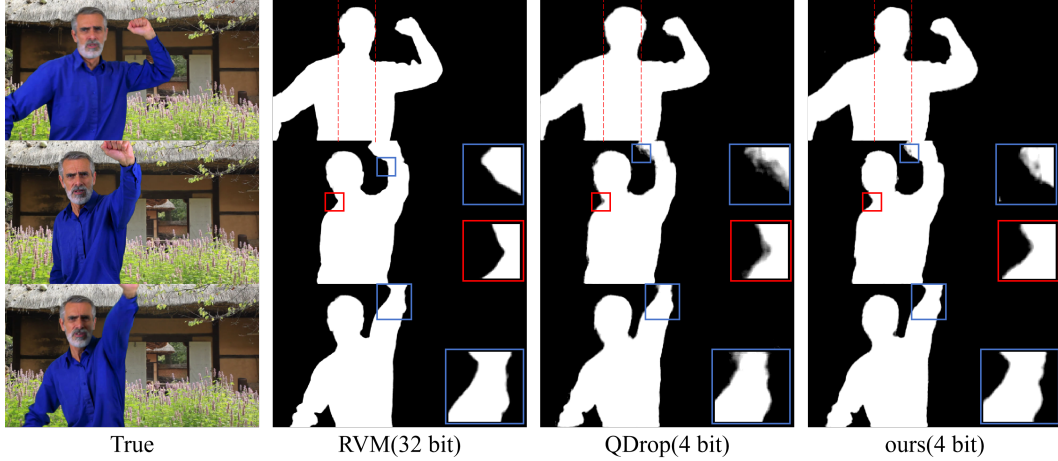


Figure 1: Visual comparison of our PTQ4VM against Full-Precision (RVM) and QDrop . Our method demonstrates significant advantages in preserving fine details and temporal coherence.

performance, it demands extensive labeled data and computational resources, which are often scarce for video matting. In contrast, Post-Training Quantization (PTQ) quantizes pre-trained models directly with minimal calibration data and no retraining, offering significant advantages in deployment efficiency. However, dedicated Post-Training Quantization research for video matting models remains nascent. In this work, we aim to systematically investigate the challenges and opportunities of applying PTQ to video matting tasks.

However, applying PTQ to complex video matting models presents challenges. Firstly, their deep topological structures and the reliance on limited calibration data often lead to unstable convergence during the PTQ calibration process. Secondly, at low bit-widths, quantization errors propagate through the network, resulting in artifacts and increased uncertainty in the output. Furthermore, recurrent structures, crucial for capturing temporal dependencies, are particularly vulnerable to quantization noise, which can destabilize learned temporal dynamics and manifest as flickering or jitter.

To address these challenges, this paper proposes a novel PTQ framework specifically designed for video matting models. To the best of our knowledge, this is the first work to systematically tackle PTQ for this task. Our framework is designed to be general, and its main contributions are as follows:

1. **A Two-Stage PTQ Strategy Combining Block-wise and Global Optimization** We initially quantize the network using block-wise optimization, which achieves fast and stable convergence while capturing critical local dependencies. Subsequently, we perform a global calibration of quantization parameters to minimize accuracy loss while preserving PTQ efficiency.
2. **Statistically-Driven Global Affine Calibration of Quantization Parameters** We observe that neglecting Batch Normalization (BN) layers[21] in standard Post-Training Quantization (PTQ) pipelines often leads to significant statistical alterations in the distributions of intermediate layer outputs. We propose a Global Affine Calibration (GAC) method that enables the network to learn a compensation for these cumulative statistical distortions.
3. **Optical Flow Assistance to Guide Post-Training Quantization** To align with the temporal and semantic characteristics of video, we innovatively introduce an Optical Flow[23] Assistance (OFA) component. This component utilizes optical flow fields computed from adjacent frames to warp the prediction of the previous frame, serving as a strong temporal and semantic prior for the current frame. Under the guidance of this component, the Post-Training Quantization (PTQ) process enhances the model’s ability to distinguish between moving foregrounds and backgrounds in complex scenes.

Our proposed framework (PTQ4VM) not only quantitatively reduces the error of existing PTQ methods on video matting tasks by 10%–20% but also achieves performance remarkably close to the

full-precision counterpart, even under challenging 4-bit quantization, while concurrently enjoying substantial  $8\times$  FLOP savings.

## 2 Related Work

**Video Matting** is significantly developed with the advent of deep learning, surpassing traditional methods[24, 25] reliant on low-level handcrafted priors in terms of accuracy and robustness. Modern video matting models often employ encoder-decoder architectures augmented with specific modules to handle temporal dependencies. For instance, some models focus on real-time image matting, showcasing progress in efficiency for single-frame tasks. Among various video matting models, RVM (Robust High-Resolution Video Matting with Temporal Guidance)[1] stands out for its effective use of temporal information via a recurrent architecture (e.g., GRU) and temporal guidance mechanisms, achieving smooth mattes for high-resolution videos. RVM strikes a good balance between accuracy, temporal consistency, and model efficiency. Compared to some larger counterparts, RVM maintains high-quality output with a relatively lightweight architecture. Consequently, we select RVM as the full-precision baseline model for our quantization study, as it is an ideal candidate for efficient practical deployment post-quantization. However, even relatively efficient models like RVM present computational and memory challenges when deployed on resource-constrained devices, underscoring the need for model compression techniques such as quantization.

**Post-Training Quantization (PTQ)** focuses on the accurate determination of the quantization parameters. MSE-based methods are foundational, optimizing  $s$  and  $z$  by minimizing the Mean Squared Error between the original floating-point tensors and their quantized counterparts using a calibration set. To further enhance PTQ performance, several advanced algorithms have been proposed. AdaRound[26] learns an optimal rounding strategy for weight quantization, adapting weights towards minimizing task loss rather than mere weight reconstruction error, proving particularly effective for very low bit-widths. BRECQ (Block Reconstruction)[27] improves upon layer-wise quantization by partitioning the network into blocks and optimizing quantization parameters per block to minimize the reconstruction error of its output, thereby better capturing inter-layer dependencies. QDrop[28] enhances model robustness to quantization perturbations by simulating quantization noise during calibration, for instance, by randomly dropping quantized versions of activations. While these PTQ techniques demonstrate strong performance on general vision tasks, their optimal combination and adaptation for the unique demands of video matting, such as integrating block-wise optimization with global calibration, specific weight adjustment strategies, and preserving temporal consistency, remain open research areas. Our work addresses these aspects by proposing a tailored PTQ pipeline.

**Optical Flow** estimation computes pixel-level motion between video frames and is widely applied in motion analysis, object tracking, video stabilization, and as input for complex video understanding tasks such as video matting. Traditional methods like Lucas-Kanade[29] rely on local constraints. Deep learning approaches, since FlowNet[30], learn optical flow end-to-end via CNNs, significantly improving accuracy and robustness. Subsequent methods, such as PWC-Net[31], introduced feature pyramids and cost volumes. Among current state-of-the-art algorithms, RAFT (Recurrent All-Pairs Field Transforms)[22] exhibits outstanding performance. The core of RAFT lies in its iterative optimization mechanism: it constructs a 4D cost volume pyramid of all-pairs correlations and iteratively updates the flow field from an initial estimate using a recurrent unit (e.g., ConvGRU). Key advantages of RAFT include its effectiveness in handling large displacements, strong generalization capabilities, and high accuracy on standard benchmarks. Its iterative nature also allows for a trade-off between accuracy and efficiency. Consequently, we select RAFT to obtain high-precision optical flow priors to assist in the temporal and semantic enhancement of video matting.

## 3 Methods

### 3.1 Preliminaries

**Weight and Activation Quantization** The fundamental principle of uniform affine quantization maps a full-precision value  $v$  (e.g., FP32) to a lower-bit integer  $v_q$  (e.g., INT8) using a scale factor  $s$  and a zero-point  $z$ :

$$v_q = \text{clip}(\text{round}(v/s + z), Q_{\min}, Q_{\max}) \quad (1)$$





### 3.2 BIQ: Block-wise Initial Quantization for Fast Convergence & Local Dependency

**Consideration of Optimization Granularity** The choice of optimization granularity is a critical factor affecting final quantization performance. When applying PTQ to models with complex architectures, quantization noise can have a significant impact. Some studies[32] indicate that efficient models, particularly those with depth-wise separable convolutions, often exhibit a significant performance drop with PTQ, sometimes even resulting in random-level performance. Our experiments also confirm that attempting direct end-to-end optimization faces challenges such as training instability and convergence difficulties. Concurrently, layer-wise calibration overlooks inter-layer dependencies and can impose high memory requirements, especially in video tasks. We ultimately opted for a block-wise partitioning strategy. Experiments indicate that block-wise optimization not only excels in computational efficiency and effectively captures crucial local dependencies but also, with appropriate block partitioning, maintains high optimization potential, striking an optimal balance between accuracy and efficiency.

**Block-wise Sequential Optimization and Parameter Learning** We partition the network into several computational blocks ( $B_i$ ), and quantize them sequentially in topological order. For the current block  $B_i$ , the input to its quantized version,  $x_{q,in}$ , is the output from preceding quantized blocks. Its full-precision counterpart receives a corresponding input,  $x_{fp,in}$ , from preceding full-precision blocks; both  $x_{q,in}$  and  $x_{fp,in}$  originate from the same raw calibration sample.

For each block  $B_i$ , we learn optimal rounding for its full-precision weights  $W$  and learn adaptive scale factors for its input activations. These quantization parameters are determined by iteratively minimizing the Mean Squared Error (MSE) between the block’s quantized output  $Y_q$  and its full-precision output  $Y_{fp}$ . This learning process is performed iteratively over the calibration data.

### 3.3 GAC: Global Affine Calibration for Statistical Deviations in PTQ

**Distributional Shift of Intermediate Outputs post-Quantization** The core issue in PTQ is the significant accuracy degradation post-quantization. We are the first to focus on the Batch Normalization (BN) layer, explaining this phenomenon from a statistical analysis perspective and highlighting the shortcomings of general PTQ frameworks.

Typical Post-Training Quantization (PTQ) frameworks initially fold Batch Normalization (BN) layers into their preceding convolutional or fully-connected layers, yielding effective weights  $W_f$ . Subsequently, these effective weights  $W_f$  undergo weight quantization.

However, we observe that during layer-wise quantization and forward propagation, the errors introduced by weight and activation quantization accumulate. This accumulation leads to a significant shift in the statistical characteristics (e.g., mean, variance, distribution shape) of intermediate layer activations  $x$  (i.e., the input to the next layer), causing them to deviate from their counterparts in the full-precision network. When these shifted activations  $x$  are processed with the folded weights  $W_f$  (which were derived based on original full-precision statistics),  $W_f$  is no longer optimal for the actual input distribution it encounters. Consequently, conventional weight quantization strategies aiming to minimize the difference between the original  $W_f$  and its quantized version  $\hat{W}_f$  become suboptimal, as they fail to account for this input distribution shift.

Critically, such accumulated distributional distortion is further reshaped and altered when passed through non-linear activation functions (e.g., ReLU, Tanh). This poses a significant challenge for subsequent activation quantization steps, as activation quantizers typically employ uniform quantization, relying on simple statistics of the activations, such as observed minimum and maximum values, to determine quantization ranges and scales. When the activation distribution has substantially deviated from its "canonical" or expected form, these statistically driven quantizers struggle to effectively compensate for distortions, potentially leading to considerable accuracy degradation.

**Global Affine Calibration of Dequantized Weights** Some works[32] have noted the bias in the quantization process and proposed pre-training Cross-Layer Equalization and Absorbing high biases. However, in our experiments, these methods did not yield any performance improvements when applied to the relatively complex models under our investigation. We attribute this primarily to the fact that in complex model architectures, quantization errors propagate layer by layer and are reshaped and amplified by non-linear operations. Consequently, merely adjusting weights quantitatively before

quantization struggles to achieve satisfactory results. Therefore, we propose a more general global linear calibration method that directly adjusts the quantized weights.

Our method is as follows: for each convolutional layer  $i$  in the network, we introduce two scalar calibration parameters for weights: a scaling factor  $\gamma_i$  and a shift factor  $\beta_i$ . These parameters are applied to the corresponding initially quantized folded weights  $W_{f,q,i}$  of that layer:

$$W'_{f,q,i} = \gamma_i W_{f,q,i} + \beta_i \quad (2)$$

Similarly, for activations  $x_i$  input to layer  $i$ , their representation after applying the quantization function, where  $s'_{a,i}$  is the activation scaling factor we optimize and  $z'_{a,i}$  is a pre-determined zero-point, can be expressed as:

$$A'_{q,i} = (\text{clip}(\lfloor x_i / s'_{a,i} \rfloor + z_{a,i}, Q_{\min,a}, Q_{\max,a}) - z_{a,i}) \cdot s'_{a,i} \quad (3)$$

where  $Q_{\min,a}$  and  $Q_{\max,a}$  are the clipping bounds for activation quantization.

The weight calibration parameters  $\{\gamma_i\}$ ,  $\{\beta_i\}$ , along with the activation scaling factors  $\{s'_{a,i}\}$  for all relevant layers, are jointly optimized by minimizing the Mean Squared Error (MSE) between the network's final predicted alpha values ( $\hat{\alpha}$ ) and the ground truth alpha mattes ( $\alpha$ ).

After calibration, these learned parameters  $\gamma_i$ ,  $\beta_i$ , and  $s'_{a,i}$  can be conveniently absorbed into the quantization parameters of the corresponding layer's weights  $W_{f,q,i}$  and activations, respectively. Thus, they typically introduce no new parameters or significant additional computational overhead during inference.

This end-to-end optimization process enables the layer-specific  $\gamma_i$ ,  $\beta_i$ , and  $s'_{a,i}$  to collaboratively learn a global compensation mechanism, systematically correcting accumulated errors and distributional shifts introduced by quantization. The method exhibits good universality as it does not rely on complex modeling of specific layers or error types but directly adjusts overall weight and activation scales and biases by optimizing the final task objective. Importantly, our global calibration mechanism can be readily applied on top of various existing PTQ methods, yielding significant performance improvements.

### 3.4 OFA: Optical Flow Assistance for Temporal-Semantic Coherence in PTQ

In video matting tasks, particularly for quantized models, merely predicting  $\alpha$  mattes frame-by-frame often fails to capture complex dynamic scenes, leading to temporal flickering or inconsistencies in the output. To further enhance the quality of predictions, we innovatively introduce an optimization method based on optical flow. Optical flow not only provides robust temporal consistency constraints by capturing pixel-level motion trajectories to smooth transitions between consecutive frames, but also assists the model in deeper semantic recognition and motion semantic understanding.

It is noteworthy that although optical flow estimation itself entails a certain computational complexity, which has precluded its direct integration into training scenarios requiring extensive iterations (such as training full-precision models from scratch or Quantization-Aware Training, QAT), Post-Training Quantization (PTQ) typically requires only a very small calibration dataset. This characteristic of low data demand and short training iteration cycles makes the application of optical flow for temporal and semantic enhancement computationally feasible and well-targeted within the PTQ framework.

**Method** The core idea is to utilize inter-frame motion information to impose temporal constraints on  $\alpha$  matte predictions across consecutive frames. Optical flow captures pixel-level motion trajectories between adjacent input frames  $I_{t-1}$  and  $I_t$ . By computing the optical flow field  $F_{t-1 \rightarrow t}$  from  $I_{t-1}$  to  $I_t$ , the  $\alpha$  matte  $\hat{\alpha}_{t-1}$  predicted by the model for the previous frame can be effectively warped to the coordinate system of the current frame, yielding a motion-compensated estimate for the current frame's  $\alpha$  matte:  $\tilde{\alpha}_t = \text{Warp}(\hat{\alpha}_{t-1}, F_{t-1 \rightarrow t})$ .

This flow-warped matte,  $\tilde{\alpha}_t$ , serves as a strong temporal prior for the current frame's true  $\alpha$  matte. We encourage the model's direct prediction for the current frame,  $\hat{\alpha}_t = M_Q(I_t)$  (where  $M_Q$  is the quantized model), to align with this motion-compensated prior  $\tilde{\alpha}_t$ . This alignment is quantified using an L1 loss, which is incorporated as a regularization term into the model's optimization objective, typically for fine-tuning parameters obtained from Phase 1 or during a dedicated PTQ optimization. By pre-computing and storing the optical flow  $F$  on the small calibration set, the computation of  $\mathcal{L}_{\text{OFA}}$  becomes very concise and rapid. This lightweight OFA component further enhances the superiority and efficiency of our PTQ framework.

**Procedure and Loss Function** Given two consecutive frames  $I_{t-1}$  and  $I_t$  from a video sequence:

1. **Optical Flow Estimation:** Compute the optical flow field  $F_{t-1 \rightarrow t}$  from  $I_{t-1}$  to  $I_t$  using the RAFT algorithm.
2. **Previous Frame Alpha Prediction:** Obtain the model’s predicted alpha matte for the previous frame,  $\hat{\alpha}_{t-1} = M_Q(I_{t-1})$ .
3. **Alpha Warping:** Warp  $\hat{\alpha}_{t-1}$  using the estimated flow field  $F_{t-1 \rightarrow t}$  to obtain the motion-compensated alpha matte:  $\tilde{\alpha}_t = \text{Warp}(\hat{\alpha}_{t-1}, F_{t-1 \rightarrow t})$ .
4. **Current Frame Alpha Prediction:** Obtain the model’s direct prediction for the current frame,  $\hat{\alpha}_t = M_Q(I_t)$ .
5. **Optical Flow Assisted Loss:** Calculate the L1 distance between  $\hat{\alpha}_t$  and  $\tilde{\alpha}_t$  to define the Optical Flow Assisted (OFA) loss:  $\mathcal{L}_{\text{OFA}} = \|\hat{\alpha}_t - \tilde{\alpha}_t\|_1$

This loss term  $\mathcal{L}_{\text{OFA}}$  is incorporated into the network’s overall optimization objective to guide the model (or during a quantization parameter fine-tuning stage) towards generating more temporally coherent and semantically accurate alpha mattes.

## 4 Experiments

**Data Construction** Our calibration set is very small, consisting of only 256 images sampled from the VM dataset[10] (4 frames from each of 64 distinct video clips). Our evaluation datasets include the VM video matting dataset and the D646 image matting dataset[34]. Notably, D646 is an image matting dataset unseen by the model during training, which we use to further validate the generalization ability and overall performance of the quantized model on matting tasks.

**Evaluation Metrics** We assess the quality of the alpha matte ( $\alpha$ ) using standard video/image matting evaluation metrics, including Sum of Absolute Differences (SAD), Mean Squared Error (MSE), spatial Gradient error (Grad), and Connectivity error (Conn). For the video matting (VM) dataset, we also measure temporal coherence using the Deviation of Temporally Smoothed Alpha Differences (DTSSD).

**Implementation Details** We quantize all convolutional and fully-connected layers (if any) in the model. In this study, the primary quantization bit-width range explored is 4 to 8 bits (4-8bit). During the first stage, Block-wise Initial Quantization (BIQ), we define components from the original RVM model, such as InvertedResidual, LRASPP, BottleneckBlock, UpsamplingBlock, OutputBlock, and Projection, as independent optimization blocks. During the second stage, we perform global affine fine-tuning on the pre-trained quantized model, concurrently guided and constrained by the OFA component.

**Compared Methods** To validate the effectiveness of our method, we select several representative PTQ algorithms from the current field as comparison baselines, including: naive quantization based on minimizing Mean Squared Error (MSE-based Quantization), BRECQ[27], and QDrop[28](SOTA). We performed extensive parameter tuning for each comparison method to ensure they achieve their respective optimal performance levels, thereby guaranteeing a fair comparison.

### 4.1 Main Results

As shown in Table 1, our PTQ method demonstrates significant advantages across all evaluation metrics on both the VM and D646 datasets. Under the 8-bit quantization setting (W8A8), our method achieves performance comparable to, and in some metrics even superior to, the FP32 full-precision model. In the more challenging 4-bit quantization scenario, where many mainstream PTQ methods exhibit substantial performance degradation or even collapse, our method still maintains satisfactory matting quality and temporal coherence, significantly outperforming other compared methods. For instance, under the W4A4 setting on the VM dataset, our method shows a reduction of approximately 20% in various alpha error metrics compared to the next best method. This robustness at very low bit-widths highlights the superiority of our overall quantization framework in handling complex models and error accumulation. Particularly noteworthy is the performance on the D646 dataset.

Table 1: Quantitative comparison of our PTQ method against the FP32 baseline. Results for FLOPs, Params, and metrics are to be filled by the user. Lower values are better for all metrics. MSE for Alpha and FG is reported  $\times 10^{-3}$ .

Dataset	Method	#Bit	#FLOPs (G)↓	#Param (MB)↓	Alpha ( $\alpha$ )					FG	
					MAD↓	MSE↓	Grad↓	Conn↓	DTSSD↓	MSE↓	
VM 512x288	RVM (FP32 Baseline)	W32A32	4.57	14.5	6.08	1.47	0.88	0.41	1.36	-	
	MSE	W8A8	1.14	3.63	6.36	1.43	1.13	0.45	1.63	-	
	BRECQ	W8A8	1.14	3.63	6.17	<b>1.27</b>	1.05	0.42	1.76	-	
	QDrop	W8A8	1.14	3.63	6.24	1.54	0.96	0.44	1.49	-	
	Our PTQ RVM	W8A8	1.14	3.63	<b>6.03</b>	1.29	<b>0.95</b>	<b>0.41</b>	<b>1.46</b>	-	
	MSE	W4A8	0.76	2.42	168.22	158.09	14.25	24.34	4.53	-	
	BRECQ	W4A8	0.76	2.42	28.67	19.94	7.47	3.84	3.35	-	
	QDrop	W4A8	0.76	2.42	11.72	5.28	3.75	1.30	2.55	-	
	Our PTQ RVM	W4A8	0.76	2.42	<b>10.77</b>	<b>4.54</b>	<b>3.49</b>	<b>1.15</b>	<b>2.51</b>	-	
	MSE	W4A4	0.57	1.81	189.21	184.38	15.08	27.40	<b>3.81</b>	-	
	BRECQ	W4A4	0.57	1.81	168.34	161.61	15.27	24.36	5.10	-	
	QDrop	W4A4	0.57	1.81	24.36	18.02	8.92	3.16	4.70	-	
	Our PTQ RVM	W4A4	0.57	1.81	<b>20.33</b>	<b>13.80</b>	<b>7.48</b>	<b>2.57</b>	4.63	-	
D646 512x512	RVM (FP32 Baseline)	W32A32	8.12	14.5	6.63	1.91	2.43	1.60	0.80	2.54	
	MSE	W8A8	2.03	3.63	8.03	2.56	3.22	1.97	1.10	2.77	
	BRECQ	W8A8	2.03	3.63	7.25	2.33	2.89	1.77	1.07	<b>2.53</b>	
	QDrop	W8A8	2.03	3.63	7.19	<b>2.20</b>	<b>2.85</b>	1.77	0.98	2.58	
	Our PTQ RVM	W8A8	2.03	3.63	<b>7.14</b>	2.23	2.92	<b>1.76</b>	<b>0.92</b>	2.58	
	MSE	W4A8	1.35	2.42	234.09	228.48	29.43	61.19	<b>1.38</b>	26.61	
	BRECQ	W4A8	1.35	2.42	60.67	50.88	18.22	15.98	1.94	16.56	
	QDrop	W4A8	1.35	2.42	19.93	11.89	10.35	5.28	1.62	<b>4.69</b>	
	Our PTQ RVM	W4A8	1.35	2.42	<b>18.77</b>	<b>11.14</b>	<b>9.94</b>	<b>4.97</b>	1.61	4.97	
	MSE	W4A4	1.02	1.81	234.11	228.50	29.48	61.19	<b>1.49</b>	11.98	
	BRECQ	W4A4	1.02	1.81	216.46	208.53	30.24	56.64	3.77	90.92	
	QDrop	W4A4	1.02	1.81	47.91	40.15	20.85	12.60	2.36	9.13	
	Our PTQ RVM	W4A4	1.02	1.81	<b>46.73</b>	<b>38.63</b>	<b>18.54</b>	<b>12.26</b>	3.52	<b>8.68</b>	

Since our calibration set is derived entirely from the VM video dataset, D646 represents uncalibrated image matting data for the model. Our method still achieves leading quantization performance on this dataset, which strongly demonstrates the good generalization ability of the proposed method, whose core calibration strategies can be effectively transferred to different data distributions and task characteristics. Overall, our method preserves the accuracy and temporal quality of video matting while substantially compressing model size and reducing computational complexity, providing robust support for the practical application of PTQ techniques in complex video processing tasks.

We also provide visual comparisons. As shown in Figure 3a, our training framework enhances matting accuracy, exhibiting better performance on intricate curve and motion details. Figure 3b demonstrates the improvement in video semantic understanding due to our framework. Even full-precision models sometimes fail to distinguish similar static background interference, but our model accurately identifies the moving foreground, which also corroborates the guiding role of the OFA component.

## 4.2 Ablation Studies

**Effectiveness and Generality Analysis of Global Affine Calibration (GAC)** We apply the GAC module independently to two state-of-the-art PTQ algorithms, BRECQ and QDrop. Specifically, we first obtain the quantized models generated by BRECQ and QDrop at different bit-widths, and then apply GAC for further fine-tuning, with the optimization objective consistent with that of Stage 2 in our complete framework.

As shown in Table 2, GAC significantly enhances the performance of both BRECQ and QDrop across various metrics under low bit-width settings, particularly for W4A4.

Notably, the performance gain from GAC is particularly significant for BRECQ. After applying GAC, nearly all metrics for BRECQ improve substantially, bringing its performance to a level comparable with QDrop without GAC. This phenomenon is quite insightful, offering a new perspective for understanding methods like QDrop that optimize by simulating quantization noise. QDrop learns

Table 2: Quantitative comparison of our PTQ method against the FP32 baseline. Results for FLOPs, Params, and metrics are to be filled by the user. Lower values are better for all metrics. MSE for Alpha and FG is reported  $\times 10^{-3}$ .

Dataset	Method	#Bit	#FLOPs (G)↓	#Param (MB)↓	Alpha ( $\alpha$ )					FG MSE↓
					MAD↓	MSE↓	Grad↓	Conn↓	DTSSD↓	
VM 512x288	BRECQ	W4A8	0.76	2.42	28.67	19.94	7.47	3.84	3.35	-
	BRECQ+GAC	W4A8	0.76	2.42	14.91	7.21	3.37	1.73	2.50	-
	BRECQ+GAC+OFA	W4A8	0.76	2.42	13.18	6.78	3.25	1.48	2.59	-
	QDrop	W4A8	0.76	2.42	11.72	5.28	3.75	1.30	2.55	-
	QDrop+GAC	W4A8	0.76	2.42	10.98	4.43	3.36	1.17	2.46	-
	QDrop+GAC+OFA	W4A8	0.76	2.42	10.77	4.54	3.49	1.15	2.51	-
	BRECQ	W4A4	0.57	1.81	168.34	161.61	15.27	24.36	5.10	-
	BRECQ+GAC	W4A4	0.57	1.81	50.75	39.84	10.44	7.11	8.01	-
	BRECQ+GAC+OFA	W4A4	0.57	1.81	46.16	27.29	7.29	5.17	3.15	-
	QDrop	W4A4	0.57	1.81	24.36	18.02	8.92	3.16	4.70	-
	QDrop+GAC	W4A4	0.57	1.81	22.01	11.85	6.90	2.80	3.96	-
	QDrop+GAC+OFA	W4A4	0.57	1.81	20.33	13.80	7.48	2.57	4.63	-

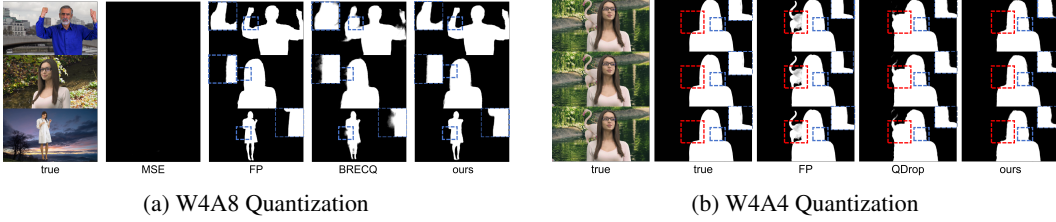


Figure 3: Comparison of PTQ4VM with Ground Truth (true), Full-Precision (FP) RVM, MSE, BRECQ, and QDrop under (a) W4A8 and (b) W4A4 quantization. Our method demonstrates superior accuracy and video understanding capabilities.

weights and quantization parameters robust to statistical deviations through random perturbations during training, whereas GAC directly compensates for the statistical deviations introduced by quantization via a simple linear transformation globally.

**Effectiveness of the Optical Flow-Assisted (OFA) Component** We investigate the potential benefits of the OFA component for the second-stage calibration of existing PTQ methods. As indicated in Table 2, when the OFA component is integrated into the second-stage calibration process for both BRECQ and QDrop, further improvements in accuracy are observed for both methods. This suggests that the temporal priors provided by OFA can effectively guide the optimization within our own framework.

**Limitation** Finally, our method cannot fully achieve the detail-capturing capability of full-precision models, and the degradation of model representational capacity remains a challenge under extremely low bit-widths (e.g., 1-2 bits).

## 5 Conclusion

To the best of our knowledge, this paper presents the first effective Post-Training Quantization (PTQ) framework specifically tailored for the video matting task. We have proposed a general multi-stage quantization strategy that first performs initial quantization via block-wise optimization, followed by a layer-wise linear weight calibration to refine quantization parameters. Furthermore, we innovatively introduced an Optical Flow-Assisted (OFA) component, which not only significantly enhances the temporal consistency of the quantized model over long video sequences but also improves its video semantic understanding capabilities. Experiments demonstrate that our method can maintain matting quality comparable to full-precision models while substantially reducing model computation and storage requirements, exhibiting superior robustness and generalization even at very low bit-widths. This work offers a viable solution for the practical deployment of video matting models on resource-

constrained devices and provides insights for future PTQ research in complex video processing tasks. This methodology also exemplifies an effective application of optical flow, showcasing its utility in regularizing the fine-tuning of quantized models for temporally coherent video processing.

## References

- [1] S. Lin, L. Yang, I. Saleemi, and S. Sengupta, “Robust high-resolution video matting with temporal guidance,” in *Proceedings of the IEEE/CVF Winter Conference on Applications of Computer Vision*, 2022, pp. 238–247.
- [2] Y. Aksoy, T. Ozan Aydin, and M. Pollefeys, “Designing effective inter-pixel information flow for natural image matting,” in *Proceedings of the IEEE conference on computer vision and pattern recognition*, 2017, pp. 29–37.
- [3] X. Bai and G. Sapiro, “A geodesic framework for fast interactive image and video segmentation and matting,” in *2007 IEEE 11th International Conference on Computer Vision*. IEEE, 2007, pp. 1–8.
- [4] Q. Chen, D. Li, and C.-K. Tang, “Knn matting,” *IEEE transactions on pattern analysis and machine intelligence*, vol. 35, no. 9, pp. 2175–2188, 2013.
- [5] Y.-Y. Chuang, B. Curless, D. H. Salesin, and R. Szeliski, “A bayesian approach to digital matting,” in *Proceedings of the 2001 IEEE Computer Society Conference on Computer Vision and Pattern Recognition. CVPR 2001*, vol. 2. IEEE, 2001, pp. II–II.
- [6] X. Feng, X. Liang, and Z. Zhang, “A cluster sampling method for image matting via sparse coding,” in *Computer Vision–ECCV 2016: 14th European Conference, Amsterdam, The Netherlands, October 11–14, 2016, Proceedings, Part II 14*. Springer, 2016, pp. 204–219.
- [7] J. Li, V. Goel, M. Ohanyan, S. Navasardyan, Y. Wei, and H. Shi, “Vmformer: End-to-end video matting with transformer,” in *Proceedings of the IEEE/CVF Winter Conference on Applications of Computer Vision*, 2024, pp. 6678–6687.
- [8] Y. Sun, G. Wang, Q. Gu, C.-K. Tang, and Y.-W. Tai, “Deep video matting via spatio-temporal alignment and aggregation,” in *Proceedings of the IEEE/CVF Conference on Computer Vision and Pattern Recognition*, 2021, pp. 6975–6984.
- [9] Y. Zhang, C. Wang, M. Cui, P. Ren, X. Xie, X.-S. Hua, H. Bao, Q. Huang, and W. Xu, “Attention-guided temporally coherent video object matting,” in *Proceedings of the 29th ACM International Conference on Multimedia*, 2021, pp. 5128–5137.
- [10] S. Lin, A. Ryabtsev, S. Sengupta, B. L. Curless, S. M. Seitz, and I. Kemelmacher-Shlizerman, “Real-time high-resolution background matting,” in *Proceedings of the IEEE/CVF Conference on Computer Vision and Pattern Recognition*, 2021, pp. 8762–8771.
- [11] S. Sengupta, V. Jayaram, B. Curless, S. M. Seitz, and I. Kemelmacher-Shlizerman, “Background matting: The world is your green screen,” in *Proceedings of the IEEE/CVF Conference on Computer Vision and Pattern Recognition*, 2020, pp. 2291–2300.
- [12] Z. Zhao, J. Zhang, X. Gu, C. Tan, S. Xu, Y. Zhang, R. Timofte, and L. Van Gool, “Spherical space feature decomposition for guided depth map super-resolution,” in *Proceedings of the IEEE/CVF International Conference on Computer Vision*, 2023, pp. 12 547–12 558.
- [13] Z. Zhao, J. Zhang, S. Xu, Z. Lin, and H. Pfister, “Discrete cosine transform network for guided depth map super-resolution,” in *Proceedings of the IEEE/CVF conference on computer vision and pattern recognition*, 2022, pp. 5697–5707.
- [14] Z. Zhao, J. Zhang, H. Bai, Y. Wang, Y. Cui, L. Deng, K. Sun, C. Zhang, J. Liu, and S. Xu, “Deep convolutional sparse coding networks for interpretable image fusion,” in *Proceedings of the IEEE/CVF Conference on Computer Vision and Pattern Recognition*, 2023, pp. 2369–2377.
- [15] Z. Zhao, S. Xu, J. Zhang, C. Liang, C. Zhang, and J. Liu, “Efficient and model-based infrared and visible image fusion via algorithm unrolling,” *IEEE Transactions on Circuits and Systems for Video Technology*, vol. 32, no. 3, pp. 1186–1196, 2021.
- [16] Z. Zhao, H. Bai, Y. Zhu, J. Zhang, S. Xu, Y. Zhang, K. Zhang, D. Meng, R. Timofte, and L. Van Gool, “Ddfm: denoising diffusion model for multi-modality image fusion,” in *Proceedings of the IEEE/CVF International Conference on Computer Vision*, 2023, pp. 8082–8093.



- [17] J. Yao, X. Wang, S. Yang, and B. Wang, “Vitmatte: Boosting image matting with pre-trained plain vision transformers,” *Information Fusion*, vol. 103, p. 102091, 2024.
- [18] B. Jacob, S. Kligys, B. Chen, M. Zhu, M. Tang, A. Howard, H. Adam, and D. Kalenichenko, “Quantization and training of neural networks for efficient integer-arithmetic-only inference,” in *Proceedings of the IEEE conference on computer vision and pattern recognition*, 2018, pp. 2704–2713.
- [19] M. Nagel, M. Fournarakis, R. A. Amjad, Y. Bondarenko, M. Van Baalen, and T. Blankevoort, “A white paper on neural network quantization,” *arXiv preprint arXiv:2106.08295*, 2021.
- [20] A. Gholami, S. Kim, Z. Dong, Z. Yao, M. W. Mahoney, and K. Keutzer, “A survey of quantization methods for efficient neural network inference,” in *Low-power computer vision*. Chapman and Hall/CRC, 2022, pp. 291–326.
- [21] S. Ioffe and C. Szegedy, “Batch normalization: Accelerating deep network training by reducing internal covariate shift,” in *International conference on machine learning*. pmlr, 2015, pp. 448–456.
- [22] Z. Teed and J. Deng, “Raft: Recurrent all-pairs field transforms for optical flow,” in *Computer Vision—ECCV 2020: 16th European Conference, Glasgow, UK, August 23–28, 2020, Proceedings, Part II 16*. Springer, 2020, pp. 402–419.
- [23] B. K. Horn and B. G. Schunck, “Determining optical flow,” *Artificial intelligence*, vol. 17, no. 1-3, pp. 185–203, 1981.
- [24] A. R. Smith and J. F. Blinn, “Blue screen matting,” in *Proceedings of the 23rd annual conference on Computer graphics and interactive techniques*, 1996, pp. 259–268.
- [25] Y.-Y. Chuang, A. Agarwala, B. Curless, D. H. Salesin, and R. Szeliski, “Video matting of complex scenes,” in *Proceedings of the 29th annual conference on Computer graphics and interactive techniques*, 2002, pp. 243–248.
- [26] M. Nagel, R. A. Amjad, M. Van Baalen, C. Louizos, and T. Blankevoort, “Up or down? adaptive rounding for post-training quantization,” in *International conference on machine learning*. PMLR, 2020, pp. 7197–7206.
- [27] Y. Li, R. Gong, X. Tan, Y. Yang, P. Hu, Q. Zhang, F. Yu, W. Wang, and S. Gu, “Brecq: Pushing the limit of post-training quantization by block reconstruction,” *arXiv preprint arXiv:2102.05426*, 2021.
- [28] X. Wei, R. Gong, Y. Li, X. Liu, and F. Yu, “Qdrop: Randomly dropping quantization for extremely low-bit post-training quantization,” *arXiv preprint arXiv:2203.05740*, 2022.
- [29] B. D. Lucas and T. Kanade, “An iterative image registration technique with an application to stereo vision,” in *IJCAI’81: 7th international joint conference on Artificial intelligence*, vol. 2, 1981, pp. 674–679.
- [30] A. Dosovitskiy, P. Fischer, E. Ilg, P. Hausser, C. Hazirbas, V. Golkov, P. Van Der Smagt, D. Cremers, and T. Brox, “FlowNet: Learning optical flow with convolutional networks,” in *Proceedings of the IEEE international conference on computer vision*, 2015, pp. 2758–2766.
- [31] D. Sun, X. Yang, M.-Y. Liu, and J. Kautz, “Pwc-net: Cnns for optical flow using pyramid, warping, and cost volume,” in *Proceedings of the IEEE conference on computer vision and pattern recognition*, 2018, pp. 8934–8943.
- [32] M. Nagel, M. v. Baalen, T. Blankevoort, and M. Welling, “Data-free quantization through weight equalization and bias correction,” in *Proceedings of the IEEE/CVF international conference on computer vision*, 2019, pp. 1325–1334.
- [33] R. Krishnamoorthi, “Quantizing deep convolutional networks for efficient inference: A whitepaper,” *arXiv preprint arXiv:1806.08342*, 2018.

- [34] Y. Qiao, Y. Liu, X. Yang, D. Zhou, M. Xu, Q. Zhang, and X. Wei, “Attention-guided hierarchical structure aggregation for image matting,” in *Proceedings of the IEEE/CVF Conference on Computer Vision and Pattern Recognition*, 2020, pp. 13 676–13 685.
- [35] H. Qin, L. Ke, X. Ma, M. Danelljan, Y.-W. Tai, C.-K. Tang, X. Liu, and F. Yu, “Bimattng: Efficient video matting via binarization,” *Advances in Neural Information Processing Systems*, vol. 36, pp. 43 307–43 321, 2023.

## A Technical Appendices and Supplementary Material

### A.1 Analysis of Block-wise Initial Quantization (BIQ) Convergence

As discussed in Section 3.2 of the main paper, the choice of optimization granularity is critical to the final performance of Post-Training Quantization (PTQ). This section provides experimental support for this choice by presenting the convergence curves of Alpha error) for block-wise optimization versus naive full-network quantization under different bit-width settings.

**Convergence Comparison under Various Bit-widths** We compare the convergence process of our proposed Block-wise Initial Quantization (BIQ) method against a naive full-network direct quantization approach (which attempts to optimize quantization parameters for the entire network at once to minimize MSE against the full-precision output, serving as a baseline for comparison) under two different weight-activation bit-width settings: W4A4 and W4A8. The optimization objective for both is to minimize the Mean Square Error (MSE) between the block output (for BIQ) or the final network alpha output (for full-network quantization) and their full-precision counterparts. Figure 4 illustrates the Alpha error, evaluated on the test set, versus the number of iterations for these two settings.

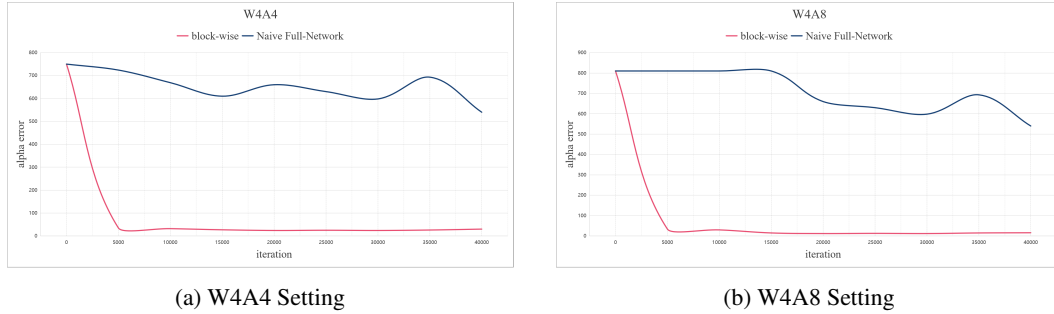


Figure 4: Convergence comparison of Alpha error for Block-wise Initial Quantization (BIQ) versus Naive Full-Network Quantization under different settings: (a) W4A4 and (b) W4A8. Evaluations are performed every 5000 iterations, and the curves are smoothed for clarity.

From these convergence curves (Figure 4), we can clearly observe:

- **Effective Convergence of BIQ versus Difficulty of Naive Full-Network Quantization** Across the tested bit-widths (W4A4 and W4A8), our Block-wise Initial Quantization (BIQ) method exhibits rapid and effective convergence. The error curve for BIQ drops quickly and stabilizes at a low level within a smaller number of iterations. In contrast, the error curve for the naive full-network quantization method shows little to no significant convergence trend, with its error values remaining persistently high, indicating the difficulty of finding an effective quantization solution by directly optimizing the entire complex network.
- **Superior Final Performance of BIQ** Due to its effective convergence, BIQ achieves a final Alpha MAD value significantly lower than what the naive full-network quantization method can reach (if the latter can be considered to have converged at all). This indicates that by optimizing block by block, we can find a far superior initial solution for the quantization parameters, more effectively capturing local dependencies and avoiding the optimization stagnation or sub-optimal solutions often encountered when attempting to optimize the entire complex network at once.

## A.2 Analysis of Affine Calibration Parameter Distributions in GAC

To further understand the mechanism by which our Global Affine Calibration (GAC) strategy enhances model performance under various quantization bit-widths (W4A4, W4A8, W8A8), this section provides a detailed analysis of the distribution characteristics of the layer-wise affine transformation parameters learned during the GAC stage: the shift factor  $\beta_i$  and the scaling factor  $\gamma_i$ . Ideally, if the initial quantization stage (e.g., after our first-stage BIQ, or after applying other PTQ methods) had perfectly corrected all statistical deviations, the learned  $\beta_i$  would be close to 0 and  $\gamma_i$  close to 1. This analysis aims to reveal the extent to which the parameters actually learned by GAC deviate from these ideal values, thereby elucidating the specific compensatory role of GAC for initially quantized models.

**Visualization of Learned Affine Parameters** Figures 5 and 6 respectively illustrate the distribution histograms of the actual  $\beta_i$  and  $\gamma_i$  parameter values learned for each convolutional layer of the RVM model, and the box plots of their deviations from the ideal values ( $\beta = 0, \gamma = 1$ ), under W4A4, W4A8, and W8A8 quantization settings.

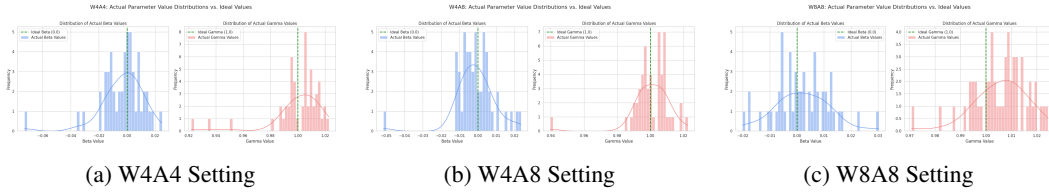


Figure 5: Histograms of learned affine calibration parameters  $\beta$  and  $\gamma$  (each subfigure typically shows distributions for both  $\beta$  and  $\gamma$ ) under different quantization settings: (a) W4A4, (b) W4A8, and (c) W8A8. The ideal  $\beta = 0$  and  $\gamma = 1$  are typically marked for reference within each panel of the subfigures.

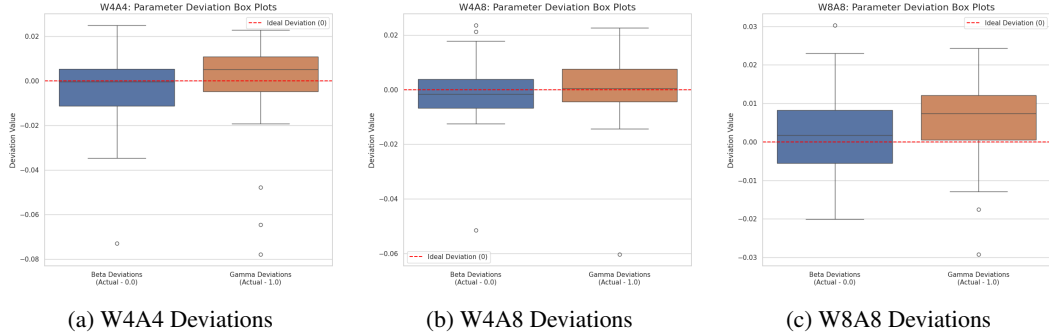


Figure 6: Box plots of deviations for learned affine calibration parameters  $\beta$  (from 0) and  $\gamma$  (from 1) under different quantization settings: (a) W4A4, (b) W4A8, and (c) W8A8.

**Analysis of Parameter Distributions and Deviations** Figures 5 and 6 collectively reveal the distribution characteristics of the learned affine calibration parameters,  $\beta_i$  and  $\gamma_i$ , and their deviations from ideal values. It is objectively observed from these figures that across all tested bit-widths (W4A4, W4A8, and W8A8), the learned parameters exhibit deviations from their ideal values of  $\beta_i = 0$  and  $\gamma_i = 1$ . Such deviations are particularly pronounced at lower bit-widths, such as W4A4, where the parameter distributions are more dispersed and the absolute range of deviations is larger.

These observed parameter deviations strongly corroborate the presence of significant residual statistical alterations (including both mean shifts and scale changes) in the weight representations after the initial quantization stage, even when advanced strategies like BIQ are employed. The GAC method, by learning non-zero shift factors  $\beta_i$  and non-unity scaling factors  $\gamma_i$ , specifically compensates for these statistical discrepancies. The more pronounced deviations at lower bit-widths further underscore the increased importance and efficacy of GAC in calibrating for larger distortions introduced by quantization, thereby explaining its crucial role in model performance recovery.

**Discussion** The preceding analysis demonstrates that even after employing advanced initial quantization strategies like BIQ, the statistical properties (mean and scale) of the quantized weights in each layer of the network still differ from an ideal state (where no further affine correction would be needed). The Global Affine Calibration (GAC) stage effectively compensates for these residual statistical deviations by learning layer-wise shift factors  $\beta_i$  and scaling factors  $\gamma_i$ . This compensation is particularly crucial for low-bit quantization and is one of the key reasons GAC can significantly enhance the performance of PTQ models. The distributions of these learned parameters, in turn, corroborate the necessity and effectiveness of performing fine-grained statistical calibration within the PTQ pipeline.

### A.3 Effectiveness of the Optical Flow-Assisted (OFA) Component in Calibration

**Experimental Setup** To further investigate the specific role of the Optical Flow-Assisted (OFA) component during the second-stage calibration process, we conducted a comparative experiment. This experiment, under the W4A4 quantization setting, compares the per-frame average Alpha error when performing joint optimization including the OFA loss term ( $\mathcal{L}_{\text{OFA}}$ ) versus optimization using only the  $\mathcal{L}_\alpha$  loss (i.e., without OFA). The experiment was conducted on the test dataset of the VM video dataset, with Alpha errors recorded frame by frame.

**Per-Frame Alpha Error Comparison and Analysis** Figure 7 illustrates the per-frame average Alpha error curves on the test dataset video sequences for models calibrated with and without the OFA component under the W4A4 quantization setting, with identical parameters used for the BIQ and GAC stages in these experiments to ensure a fair comparison.

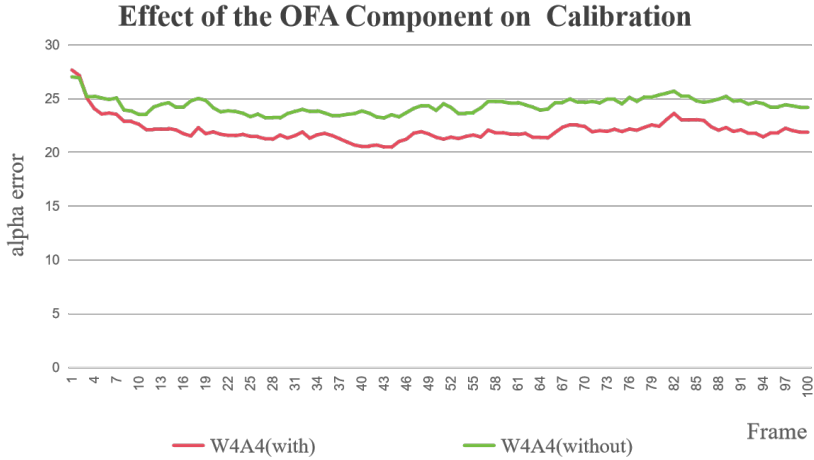


Figure 7: Per-frame average Alpha error comparison for W4A4 quantization with (red curve) and without (green curve) the OFA component on the test dataset.

As observed in Figure 7, models calibrated with the OFA component (red curve) and without it (green curve) exhibit similar Alpha errors in the initial few frames. However, as the video sequence progresses, the model incorporating the OFA component shows a distinct downward trend in average Alpha error, stabilizing at a consistently lower level. In contrast, the model without OFA maintains a relatively higher error profile throughout the later frames.

This phenomenon clearly demonstrates the effectiveness of the OFA component. Since our OFA loss,  $\mathcal{L}_{\text{OFA}}$ , is computed and applied to the optimization process starting from the second frame of a video, it leverages temporal prior information provided by optical flow to guide the PTQ calibration. This guidance not only directly encourages the model to learn more temporally coherent representations, thereby reducing prediction errors and instability in subsequent frames, but also indirectly acts as an effective regularizer, aiding the model in achieving higher overall matting accuracy.

#### A.4 Experimental setup details

**Calibration Set Construction** As mentioned in the main paper, our calibration set is very small. Specifically, we selected the first 64 video clips from the VM video dataset. For each selected clip, we uniformly sampled frames at indices [0, 2, 4, 6], resulting in a total of  $64 \times 4 = 256$  images for calibration.

**Optimization Parameter Settings** The optimization parameters for our two-stage PTQ framework are set as follows:

- **Stage 1 (BIQ - Block-wise Initial Quantization)** During this stage, for the optimization of each block, we employ the Adam optimizer with a fixed learning rate of  $4 \times 10^{-5}$ . The number of optimization iterations for each block is set to 20,000.
- **Stage 2 (GAC and OFA)** In this stage, we jointly optimize all learnable calibration parameters, which include the affine transformation parameters  $\{\gamma_i, \beta_i\}$  for GAC, the activation scaling factors  $\{s'_{a,i}\}$ , and implicitly the influence of the OFA loss. The Adam optimizer is used with a unified learning rate of  $1 \times 10^{-4}$ . The entire calibration process is run for 50 epochs. The weighting factor  $\lambda$  for the Optical Flow-Assisted loss term ( $\mathcal{L}_{\text{OFA}}$ ) is set to 0.05.

**Hardware Platform** All experiments, including model quantization, calibration, and performance evaluation, were conducted on a single NVIDIA RTX 4090 GPU equipped with 24GB of VRAM. It is worth noting that our entire PTQ calibration pipeline has low computational resource requirements, especially in terms of VRAM usage, making it well-suited for typical video matting task scenarios where pre-trained models are efficiently quantized under limited resources.